



Mesoscopic Analysis of the Mechanical Properties of Beishan Granite Based on the Equivalent Crystal Model

Wanhong Guo^{1,2,3} · Li Wang^{1,3} · Shiwen Feng¹ · Yu Zhou¹

Received: 9 July 2020 / Accepted: 15 October 2020 / Published online: 27 October 2020
© King Fahd University of Petroleum & Minerals 2020

Abstract

The internal microstructure of rock has an important influence on its macroscopic mechanical properties and fracture mechanism. In this paper, an equivalent crystal model (ECM) consisting of a bonded particle model and smooth joint model is established, which can simultaneously reflect the structure and content of mineral granules in rock. To verify the applicability and reliability of the ECM to further study the macroscopic nonlinear mechanical behaviour and fracture mechanism of rocks from a mesoscale perspective, this paper carried out numerical simulations of direct tension, uniaxial compression and triaxial compression loading using the particle flow code software, and the numerical results were compared with the test results of Beishan granite. The main research results are summarized as follows. (1) Under the condition of triaxial compression, with the increase in the confining pressure, the axial peak strain, radial peak strain, volume peak strain and post-peak residual strain of the rock all show an increasing trend. The rock exhibits an axial splitting failure mode dominated by tensile cracks and gradually changes to a shear failure mode dominated by shear cracks at an angle of approximately 45° from the loading direction. (2) Under direct tensile conditions, the failure of the rock manifests as cracks initiating from the middle of the specimen and extending approximately perpendicular to the tensile load direction, forming an approximately horizontal macroscopic crack composed of mineral granular boundaries. (3) The use of the ECM can reproduce a high ratio of the uniaxial compressive strength to the uniaxial tensile strength of the rock, and its strength characteristics show obvious nonlinear characteristics and meet the Hoek–Brown strength criterion. The rock strength and failure type obtained from the simulation are basically consistent with the test results, demonstrating the reliability of the ECM.

Keywords Equivalent crystal model · PFC program · Granite · Mesomechanism · Mechanical behaviour

1 Introduction

Rocks are natural mineral aggregates composed of one or more minerals that exist in the Earth's crust. The differences in the properties of the mesoscopic components within the rock will affect the macroscopic mechanical properties of the rock to varying degrees. Therefore, from the point of view of mesomechanics, the study of rock fracture laws under

various loads is an important basis for revealing the rock fracture failure mechanism and constitutive behaviour and is also the key to establishing the relationship between the rock's macromechanical response and mesomechanics. This has important theoretical value and guiding significance for the stability design and construction of rock mass engineering applications.

To date, the PFC program, which is based on the discontinuous medium theory, is one of the methods that can effectively analyse the macroscopic nonlinear mechanical behaviour response of rocks from a mesoscopic perspective, and the analysis results are in good agreement with the actual results [1–4]. Therefore, the PFC program has been recognized and affirmed by researchers in the field of geotechnical engineering. During the mesoscopic study of the mechanical properties of rock using the PFC program, the selected model has an important impact on the accuracy of the final research results. At present, the commonly used models in

✉ Yu Zhou
westboy85@ustb.edu.cn

¹ Key Laboratory of Ministry of Education for Efficient Mining and Safety of Metal Mine, University of Science and Technology Beijing, Beijing 100083, China

² Sinohydro Foundation Engineering Co., Ltd., Tianjin 301700, China

³ PowerChina Road Bridge Group Co., Ltd., Beijing 100048, China



PFC programs mainly include the traditional bonded particle model (BPM) [5, 6], the flat joint model (FJM) [7] and the clumped particle model (CPM) [8].

In terms of the BPM, Zhou et al. [9–11] used the traditional BPM to develop a series of studies on prefabricated fractured rock under different loads (uniaxial compression, Brazilian split and triaxial compression loads) to investigate the fracture mechanism. Based on the BPM, Park et al. [12] introduced rock structural planes and conducted a large number of rock direct shear tests. To study the deformation and strength characteristics of granite under true triaxial loading, Zhang et al. [13] conducted a three-dimensional PFC numerical simulation using the BPM. Zhang et al. [14] discussed the acoustic emission characteristics of rock under different compression loading rates based on the BPM. Although the traditional BPM is widely used, it still has the following disadvantages [15, 16]: (1) compared with natural rock, the ratio of the uniaxial compressive strength to the tensile strength (σ_c/σ_t) and internal friction angle are low; (2) the parameters m_b in the calculated Hoek–Brown strength criterion are too low. Therefore, to better solve the above problems, the FJM, which can better describe the properties of brittle rocks, has been adopted by some researchers. Zhou et al. [17] established a mesomechanical model of granite using the FJM and carried out uniaxial tensile, uniaxial compression and triaxial compression tests. A comparison with the corresponding test results confirmed the feasibility of this model. Wu et al. [18, 19] carried out uniaxial compression and Brazilian split tests based on the FJM and systematically studied the effect of the mesoscopic parameters of the 3D numerical model on the macroscopic mechanical behaviour of the specimen. Yang et al. [20] used the FJM to discuss the shear mechanical behaviour and failure mechanism of granite with structural planes in the direct shear test, and the simulation results were in good agreement with the test results. In addition, to better overcome the shortcomings of the low σ_c/σ_t BPM model, Cho et al. [21] also proposed the use of the CPM and carried out uniaxial and triaxial compression tests on brittle rock. It is worth noting that the above two models, the FJM and CPM, can solve the disadvantages of the traditional BPM to a certain extent and can more accurately simulate the nonlinear macroscopic mechanical properties of rocks; however, they fail to reflect the mineral structure and composition characteristics of rocks. This has a certain effect on accurately reproducing the mechanical behaviour of natural rocks.

Therefore, this paper establishes an ECM that can fully consider the differences of various mineral compositions in rocks to solve the deficiencies of the existing models. To verify the feasibility and accuracy of this equivalent crystalline model, based on the Beishan granite test data, this model is used to study the macroscopic mechanical properties and failure evolution mechanism of granite from a mesoscale perspective. The article first constructs an ECM based on the

BPM and SJM that can reflect the different characteristics of rock minerals. Then, direct tensile, uniaxial compression and triaxial compression tests are carried out to explore the macroscopic nonlinear mechanical behaviour and fracture mechanism of granite from a mesoscale perspective. Finally, the comparison between the numerical results and experimental results is discussed to verify the applicability and feasibility of the proposed equivalent crystalline model.

2 Experimental Design and Analysis

Granite rock samples [22–24] were taken from the Beishan pit exploration facility in Gansu Province, China's Underground Laboratory of Geological Disposal of High-level Radioactive Waste. Field observations show that the rock is greyish white, and the feldspar has a large particle size and a spotty shape. As shown in Fig. 1, the composition of the rock minerals is analysed using an optical microscope. The main components are biotite (Bt), quartz (Qtz), alkaline feldspar (Afs) and plagioclase (Pl). The average particle size of the particles is approximately 0.5 mm, 1 mm, 2 mm and 2 mm. They account for approximately 5%, 25%, 35% and 35%, respectively. According to the QAP classification triangle diagram of granite rocks, the rock is named two-long granite. According to the ISRM rock mechanics test specification, the core is processed into a cylindrical standard rock sample with a diameter of 50 mm and a height of 100 mm. Based on the QAP classification triangle diagram of granite rocks, the rock is named monzonite granite. According to the ISRM rock mechanics test specification, the core is processed into a cylindrical standard rock sample with a diameter of 50 mm and a height of 100 mm.

Five sets of conventional triaxial compression tests were carried out on granite samples, and the corresponding confining pressures (σ_3) were 5 MPa, 15 MPa, 25 MPa, 35 MPa and 45 MPa. The main test process is as follows: (1) Align the processed test piece between two rigid pads, arrange the sealing ring in the vertical direction, and then use the heat shrinkable tube to encapsulate the whole system to prevent the rock from being immersed in hydraulic oil and affecting the test results. (2) Place the test piece and the rigid pad in the centre of the pressure platform, manually adjust the indenter to contact the test piece, and then install the ring extensometer and the axial extensometer. (3) After confirming that the installation is correct, slowly lower the pressure chamber and tighten the surrounding sealing bolts to fill the pressure chamber with oil. (4) After the oil filling is completed, the confining pressure is loaded first, and the hydrostatic pressure is applied to a set value of 3 MPa/min. Then, the axial pressure is applied at a rate of 30 kN/min, and circumferential displacement control is adopted after the rock sample enters the yielding stage. The rate to quickly obtain the residual strength after

Fig. 1 Granite mineral information. **a** Optical microscope observation photographs. **b** QAP classification

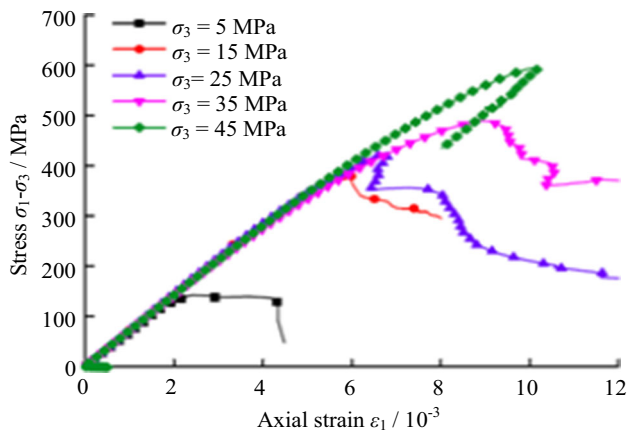
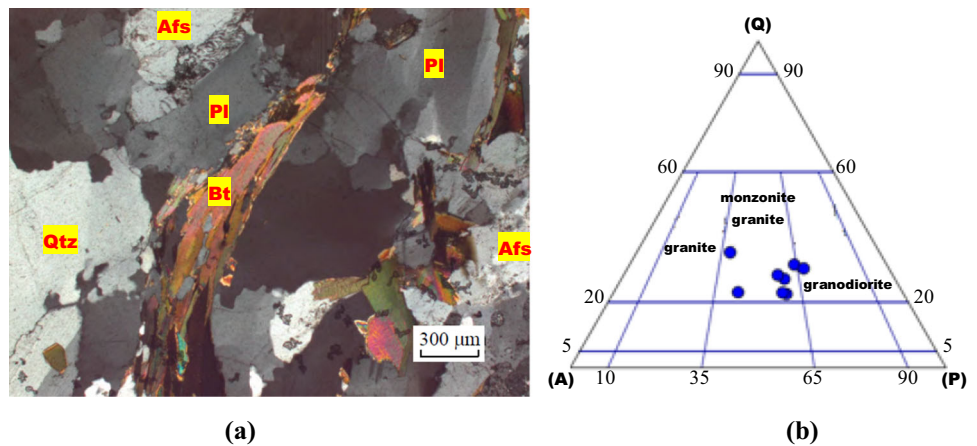


Fig. 2 The total stress–strain curves of granite under different confining pressures

reaching the peak is 0.04 mm/min, at which point the loading is changed to LVDT axial displacement control. The rate is 0.08 mm/min, until the sample is destroyed. Figure 2 shows the full stress–strain relationship curve of the granite samples under different confining pressures obtained by the conventional triaxial compression test. When the confining pressures are 5 MPa, 15 MPa, 25 MPa, 35 MPa and 45 MPa, the compressive strengths ($\sigma_1 - \sigma_3$) obtained by the tests are 156 MPa, 367 MPa, 442 MPa, 512 MPa and 589 MPa, respectively.

3 Granite Characterized by the ECM

3.1 ECM Concept

The ECM is based on the particle flow theory and built in the PFC program [25]. The ECM can truly reproduce the mineral structural characteristics and nonlinear mechanical properties of hard and brittle rock. The construction process of the ECM is as follows: (1) First, according to the type, content and structural characteristics of the mineral particles

obtained by rock scanning electron microscopy and energy spectrum analysis tests, a crystalline network structure (CNS) is constructed. (2) Then, the CNS is overlaid on the traditional BPM, and the particle model is dispersed into a crystal granular (CG) with the characteristics of the actual rock mineral granular distribution structure. In this process, the particle contact model at the CNS passing point will change to the smooth joint model (SJM). (3) Through experimental uniaxial and triaxial compression tests, macromechanical parameters such as the elastic modulus and peak strength of the sample can be obtained. Based on the macromechanical parameters, the debug-inversion method can be used to obtain the mesomechanical parameters of the SJM and BPM. Finally, the parameters are assigned to the model to build the ECM and carry out related numerical simulations. Figure 3 shows the flowchart of the ECM method.

One of the key technologies for the realization of the ECM is the SJM (Fig. 4). The SJM is a brand-new particle contact model that can be used to simulate the mechanical behaviour of the crystalline particle contact surface. The SJM simulates the behaviour of an interface regardless of the local particle contact orientations along the interface. During the modelling process, the interparticle contact orientation can be ignored. After the SJM is embedded in the particle model, all the original contact models between the adjacent particles at both ends of the CNS surface will be transformed into the SJM. The adjacent particles at both ends of the CNS surface can slide in parallel along the SJM instead of sliding along the particle surface, thereby eliminating the “bump” effect generated by the traditional particle flow simulation and finally achieving the purpose of simulating the crystal surface mechanics. The theoretical formula and calculation principle of the SJM can be found in Ref. [26].

As shown in Fig. 5, an example demonstrates that the SJM operates correctly at a single contact. It shows how one can define a local planar surface with an orientation that does not coincide with the particle contact orientation. The model consists of two unit-radius particles oriented 45° from the

Fig. 3 The approach flowchart of the ECM

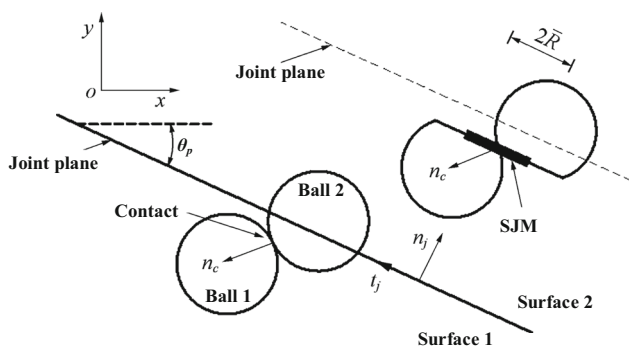
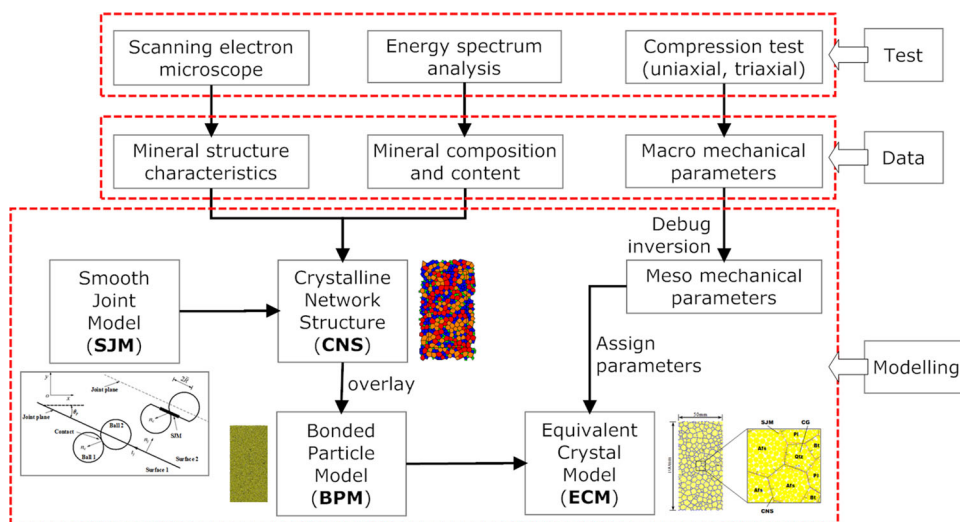


Fig. 4 Notation used to define the SJM

$y = 0$ plane. An SJM with a unit normal aligned with the global y -axis is assigned to the contact. It is assigned normal and shear stiffnesses of unity, a radius multiplier of 0.5 (to yield an area of unity), and a friction coefficient of zero. All degrees of freedom of both particles are fixed. The upper ball is first moved downward towards the $y = 0$ plane and then moved parallel with the $y = 0$ plane. The normal and shear forces with respect to the joint plane are compressive and equal to zero, respectively. The friction coefficient is set to unity, and the upper ball continues to move parallel with the $y = 0$ plane. The normal force remains constant, and the shear force magnitude increases until it equals the normal force and then remains constant.

3.2 Construction Method of the CNS

The construction process of the CNS usually includes the following four steps: (1) Establish a particle compact case that does not contain walls, where each particle has at least two contacts, and each contact connects two particles. As shown in Fig. 6a, the contact is represented by a straight line segment. (2) By closing the contact chain, the entire system can

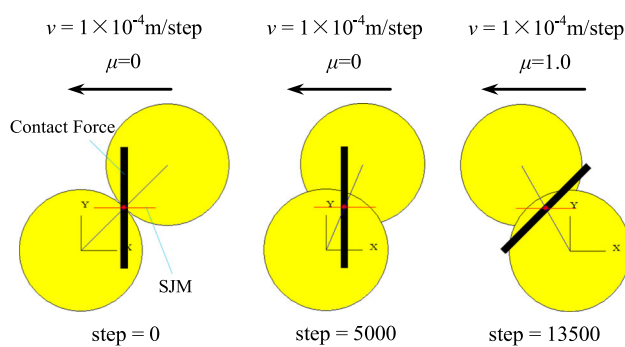


Fig. 5 An example of a working SJM

be divided into an external space and many internal spaces surrounded by the external space. The internal space is characterized by the dots in Fig. 6b, and each contact is adjacent to two spaces. The dot is the centroid of the polygon, and its position can be obtained by means of advanced mathematics. (3) The particles that are not adjacent to the external space are defined as internal particles. Each internal particle corresponds to a crystalline grid, and the boundary of the crystalline grid is the line connecting the centres of the two internal spaces, as shown in Fig. 6c. (4) A CNS is generated and its spatial geometry information is saved, as shown in Fig. 6d.

3.3 Construction of the ECM

Combined with the main mineral composition and content analysis data of the granite sample, the above CNS construction method is used, and at the same time, the CG are randomly selected according to the uniform distribution function to characterize different mineral particles. Finally, the mesostructure of the granite sample can be established and tested. The CNS with statistical similarity is shown in

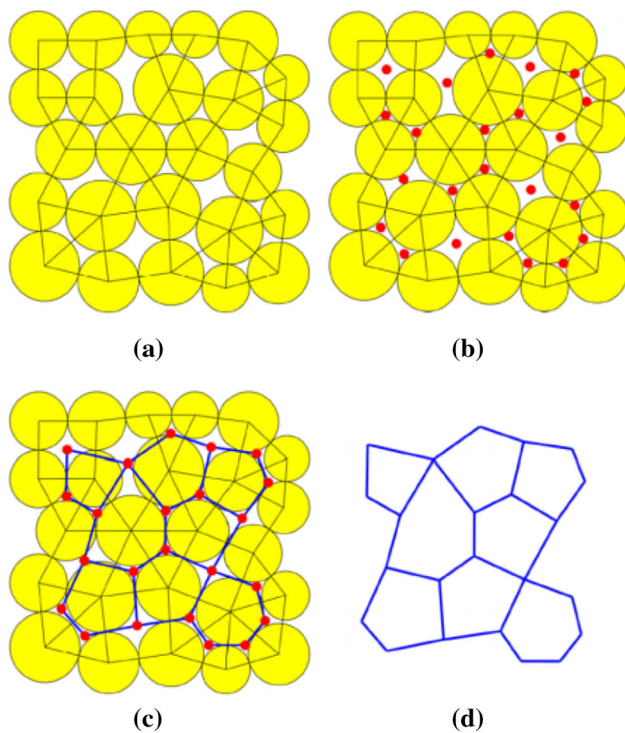


Fig. 6 Construction process of the CNS. **a** Compact particles. **b** Internal space generation. **c** Connected polygon nodes. **d** CNS generation

Fig. 7. In the figure, the four types of irregular polygons, green, blue, red and orange, represent Bt, Qtz, Afs and Pl. In the ECM, the average particle sizes of the four CG, such as Bt, Qtz, Afs and Pl, are 0.5 mm, 1 mm, 2 mm and 2 mm, respectively, and the composition ratios are 5%, 25%, 35% and 35%. The size of the BPM is 100 mm × 50 mm, which is constructed from a series of disc particles, as shown in Fig. 7. The total number of particles in the model is 9197. The minimum particle radius is $R_{min} = 0.30$ mm, the maximum radius is $R_{max} = 0.50$ mm, and the particle radius adopts a Gaussian distribution. Through cyclic calculations, a compact and extruded particle model is generated to ensure that there are more than three particles in contact with each particle.

In view of the CNS and the mechanical properties of the CG, the mesomechanical parameters of the SJM and the BPM are used to characterize the properties in this paper. For the calculation method of a discontinuous medium, there is a high degree of nonlinearity between the rock macromechanical parameters and mesomechanical parameters, and the relationship between them cannot be expressed by a definite mathematical expression. For example, for the particle flow program PFC, which uses a particle generation calculation model, the selection of the mesomechanical parameters of the particles and their bonding must be carried out by establishing a numerical sample model of the particles and assigning the assumed mesomechanical parameters to the numerical sample test. The calculated macroscopic mechan-

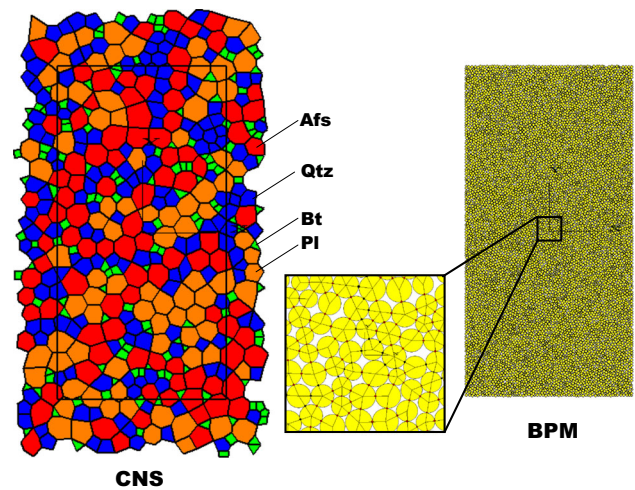


Fig. 7 Crystal network structure (CNS) and bonded particle model (BPM)

ical parameters of the sample are compared with the results of the experimental data. By continuously adjusting the mesomechanical parameters, when the calculated results are basically consistent with the test results, the mesomechanical parameters of the group of samples can be applied to other calculation models. This calibration process can be called the debug-inversion method, and it mainly includes matching the macroscopic elastic modulus, peak strength, crack initiation stress and post-peak properties of the numerical sample and the experimental sample [2–9, 25].

After repeated debugging and matching, the mechanical characteristics of the experimental granite can be described more accurately when the parameters of the SJM in Table 1 and the mesomechanical parameters of the BPM in Table 2 are used. Among them, the normal stiffness \bar{k}_n and tangential stiffness \bar{k}_s of the SJM are related to the normal stiffness k_n and tangential stiffness k_s of the particle contact and the normal stiffness \bar{k}^n and tangential stiffness \bar{k}^s parallel bond and are determined by formula (1):

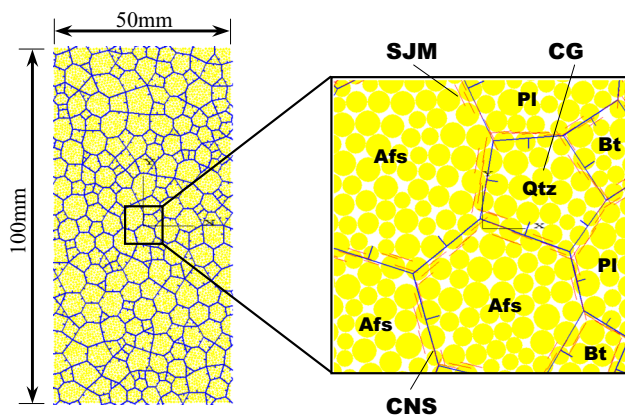
$$\begin{cases} \bar{k}_n = (k_n/A) + \bar{k}^n \\ \bar{k}_s = (k_s/A) + \bar{k}^s \\ A = 2\bar{R}t, t = 1 \end{cases} \quad (1)$$

where A is the cross-sectional area of the SJM; t is the thickness of the disc particles; \bar{R} is the contact radius for the SJM; and $\bar{R} = \bar{\lambda} \min(R^{(A)}, R^{(B)})$, where $R^{(A)}$ and $R^{(B)}$ are the radii of the two contact particles. On this basis, the final value of the stiffness of the SJM needs to be multiplied by the correlation coefficient (I_n and I_s) to characterize the weakening effect of the stiffness of the SJM.

After the construction of the CNS and the BPM is completed, the CNS is overlaid on the BPM. It should be noted that in the BPM, the particle contact model where the CNS passes will be immediately changed to the SJM, as shown in

Table 1 Mesomechanical parameters of the SJM

Correlation coefficients of the stiffness		Tensile strength σ_b (MPa)	Cohesive force of the bonding system C_b (MPa)	Friction angle of the bonding system ϕ_b ($^\circ$)
Normal I_n	Tangential I_s			
0.55	0.55	0.6	120	55

**Fig. 8** Equivalent crystal model (ECM)

Figs. 4 and 5. For the CNS and the CG, the SJM and the BPM are given mesomechanical parameters. Finally, an ECM that can reflect the structural characteristics of granular granite minerals has been constructed, as shown in Fig. 8.

3.4 Numerical Experimental Loading Scheme

In this paper, numerical experiments are carried out on uniaxial tensile, uniaxial compression and triaxial compression specimens of the granite ECM constructed above. Among them, the confining pressure of the triaxial compression test is set to 5 MPa, 15 MPa, 25 MPa, 35 MPa and 45 MPa, based on the principle of the servo mechanism, by continuously adjusting the wall rate to keep the confining pressure constant. In the calculation process, to ensure the pseudostatic loading state, the loading rate needs to be sufficiently small, where the axial compression loading rate is set to 1.0 and the axial tensile loading rate is set to 0.1.

4 Calculation Results and Analysis

4.1 Strength Characteristics

Figure 9 shows the compressive stress–strain (including the axial strain, radial strain and volumetric strain) curves of the ECM under different confining pressures. The axial stress–axial strain curves show obvious elasticity, yielding, strain softening and residual stages. Since the existence of micro-cracks or pores is not considered in the model, the

curve does not show a clear initial compaction stage. When the confining pressure is 0 MPa (that is, under uniaxial compression), the ECM shows obvious brittle failure characteristics, specifically as the axial stress–strain curve suddenly sharpens after the peak strength ($\sigma_1 = 98$ MPa) declines. With the increase in the confining pressure (5–45 MPa), the ultimate compressive strength ($\sigma_1 - \sigma_3$) of the ECM increases from 156 to 589 MPa, with an increase of 2.7 times. When the confining pressures are 5 MPa, 15 MPa, 25 MPa, 35 MPa and 45 MPa, the calculated compressive strengths ($\sigma_1 - \sigma_3$) are 209 MPa, 337 MPa, 417 MPa, 506 MPa and 568 MPa, respectively. This is approximately consistent with the results obtained from the laboratory tests of Beishan granite (Fig. 2). At the same time, the axial peak strain, radial peak strain, volume peak strain and post-peak residual strain of the model also showed an increasing trend with increasing confining pressure. When the confining pressure is low (15 MPa), the ECM shows obvious brittle failure characteristics. As the confining pressure increases, the stress–strain curve of the model gradually shows strain softening. Therefore, it can be concluded that as the confining pressure increases, the failure characteristics of the ECM change from brittle failure at a low confining pressure to ductile failure at a high confining pressure, indicating that increasing the confining pressure can improve the granite pressure-bearing capacity. This is in agreement with the laboratory test results. In addition, from the volume stress–strain curve, it can be found that with increasing confining pressure, the ECM expansion phenomenon is gradually suppressed.

The direct tensile stress–strain curve and the final tensile failure mode of the ECM are shown in Fig. 10. The peak tensile strength of this model is 3.5 MPa, and the corresponding peak tensile strain is approximately 0.1×10^{-3} . After the ECM reaches the peak tensile stress, the tensile stress–strain curve drops sharply, showing brittle tensile failure characteristics. From the final failure mode of the ECM, it can be seen that the crack starts at the middle of the model and expands approximately perpendicular to the tensile loading direction and eventually forms an approximately horizontal macroscopic crack composed of mineral particle boundaries.

To further analyse the strength characteristics of Beishan granite based in the ECM, the commonly used generalized Hoek–Brown strength criterion [27] is used to fit the peak

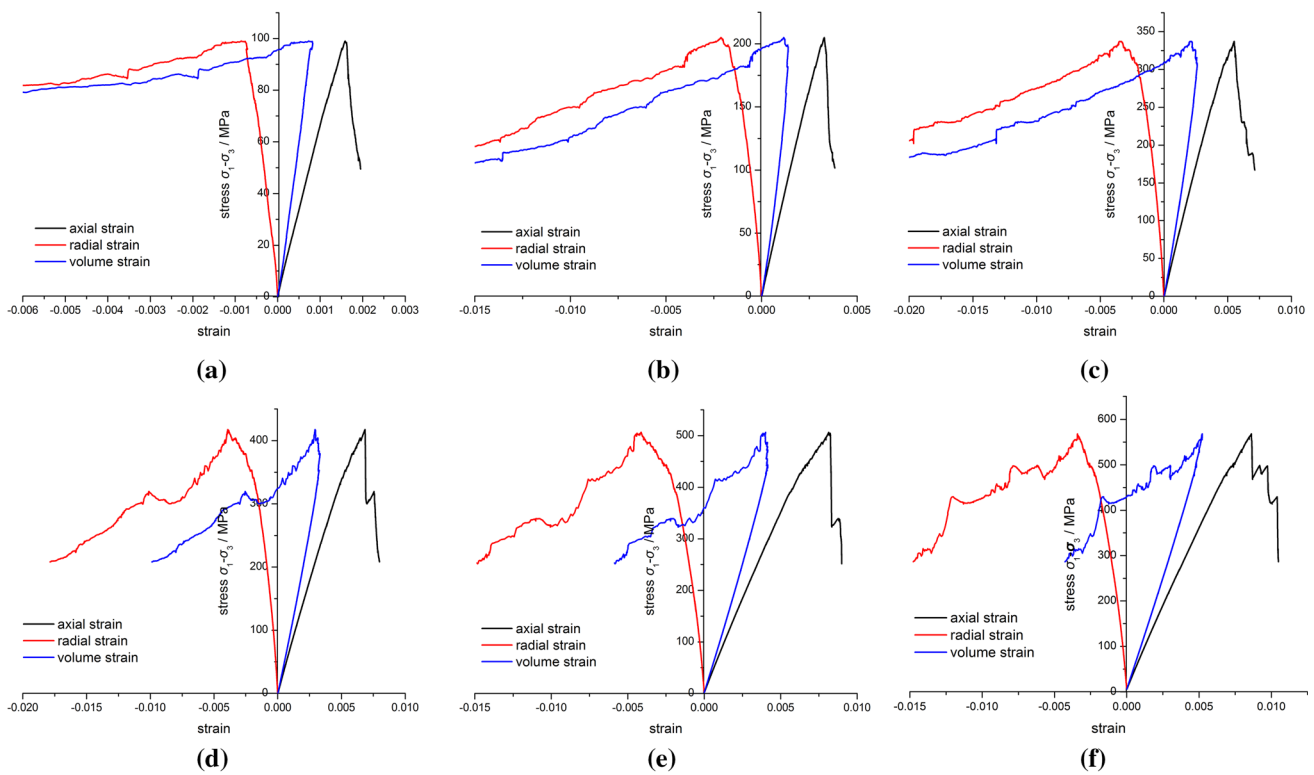


Fig. 9 The compressive stress–strain curve of the ECM under different confining pressures. **a** 0 MPa. **b** 5 MPa. **c** 15 MPa. **d** 25 MPa. **e** 35 MPa. **f** 45 MPa

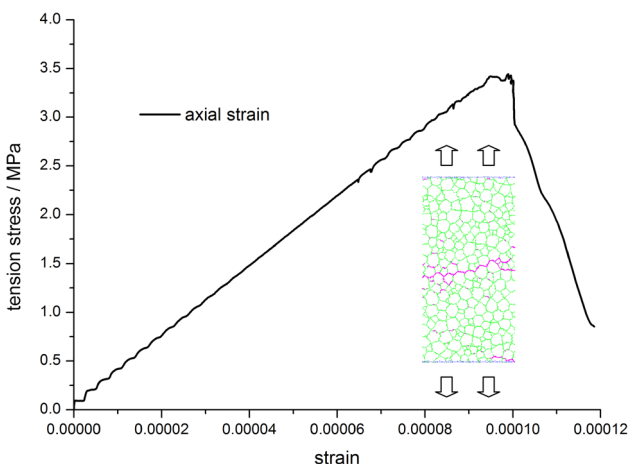


Fig. 10 The direct tensile stress–strain curve of the ECM

stress of the ECM. The specific expression of the generalized Hoek–Brown strength criterion is as follows:

$$\sigma_1 = \sigma_3 + \sigma_c \left(m_b \frac{\sigma_3}{\sigma_c} + s \right)^a \tag{2}$$

where σ_c is the uniaxial compressive strength of the rock, m_b is the strength parameter of the rock, s is the degree of rock fragmentation (value is 0–1) and a is the curvature parameter of the envelope.

According to the results in Figs. 9 and 10, it is easy to obtain the direct tensile strength, uniaxial compressive strength and triaxial compressive strength under different confining pressures. Therefore, based on the calculated data, the Hoek–Brown strength curve of the equivalent crystalline model can be fitted, as shown in Fig. 11. The specific function expression of the fitting curve is as follows:

$$\sigma_1 = \sigma_3 + 98 \left(70.86 \frac{\sigma_3}{98} + 1.0063 \right)^{0.4769} \tag{3}$$

From formula (3), the calculated Hoek–Brown strength criterion parameters, such as m_b , s and a , are 70.86, 1.0063 and 0.4769, respectively. The coefficient of determination (R^2) of the fitting function is 0.9996, indicating that the curve fitting is very accurate. It can be seen from Fig. 11 that the numerical calculation strength of the direct tensile test, uniaxial compression test and triaxial compression test based on the ECM are consistent with the experimental results. At the same time, the calculated strength of granite also meets the expression of the Hoek–Brown strength criterion. In addition, the ratio of the uniaxial compressive strength to the direct tensile strength obtained by the ECM is $\sigma_c/\sigma_t = 98 \text{ MPa}/3.5 \text{ MPa} = 28$. These results show that, on the one hand, the ECM can exhibit brittle characteristics of rock; on the other hand, the calculated mechanical behaviour of the ECM conforms to the nonlinear change law of the natural rock.

Table 2 Mesomechanical parameters of the BPM

CG	BPM density $\rho/(\text{kg}/\text{m}^3)$	Friction coefficient between grains μ	Particle elastic modulus E_c (GPa)	Stiffness ratio of the particle k_n/k_s	Parallel bond radius factor $\bar{\lambda}$	Contribution factor of the parallel bond β	Elastic modulus of the parallel bond \bar{E}_c (GPa)	Stiffness ratio of the parallel bond k^n/k^s	Tensile strength of the parallel bond $\bar{\sigma}_c$ (MPa)	Cohesion of the parallel bond \bar{c} (MPa)	Friction angle of the parallel bond ϕ ($^\circ$)
Biotite (Bt)	2500	0.5	40	2.5	1.0	1.0	40	2.5	400	800	20
Quartz (Qtz)	3000	0.5	80	2.5	1.0	1.0	80	2.5	600	1200	40
Alkaline feldspar (Afs)	2750	0.5	60	2.5	1.0	1.0	60	2.5	500	1000	30
Plagioclase (Pl)	2750	0.5	60	2.5	1.0	1.0	60	2.5	500	1000	30

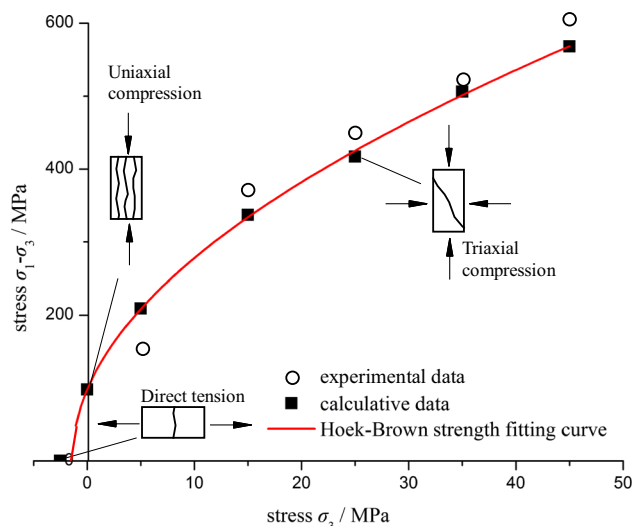


Fig. 11 Hoek–Brown strength fitting curve of the ECM

4.2 Fracture Mechanism

Figure 12 depicts the final failure mode of the ECM under different confining pressures ($\sigma_3 = 0$ MPa, 5 MPa, 15 MPa, 25 MPa, 35 MPa and 45 MPa). The pink and black lines on the CG boundary in Fig. 12 represent the tensile cracks and shear cracks caused by the SJM fractures. Tensile cracks are caused by the fracture of the parallel bonding model. The red line within the CG represents the tensile crack caused by the fracture of the parallel bond between the particles inside the CG.

When the confining pressure is 0 MPa, the failure of the ECM is mainly due to the tensile cracks generated by the SJM fracture between the CG, accompanied by a small number of shear cracks. Under this condition, the ultimate failure mode of the ECM shows a split failure mode mainly parallel to the loading direction, which is dominated by tensile cracks.

When the confining pressure is 5 MPa and 15 MPa, in addition to the tensile cracks and shear cracks caused by the SJM fracture between the CG, the local area shows a small amount of tensile cracks caused by the bond fracture of the CG internal particles. However, the ECM is still dominated by the split failure mode.

As the confining pressure continues to increase, that is, when the confining pressure reaches 25 MPa and 35 MPa, more tensile cracks caused by internal bond fracture of the CG begin to appear in the model, and the final failure mode of the ECM gradually shows shear failure with axial loading at a certain angle. The reason for this phenomenon is that under a high confining pressure, the micro-cracks are caused by the bond fracture between the particles inside the CG and the increase in the shear cracks caused by the fracture of the SJM on the boundary of the CG. The final model shows a macroshear failure mode.

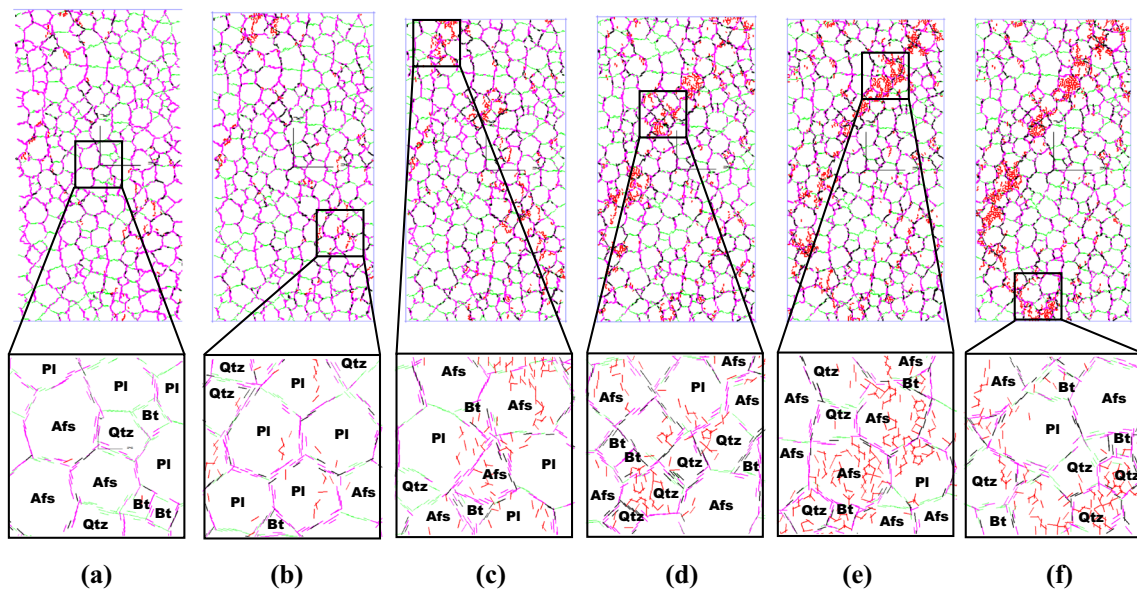


Fig. 12 The ultimate failure mode of the ECM under different confining pressures. a 0 MPa. b 5 MPa. c 15 MPa. d 25 MPa. e 35 MPa. f 45 MPa

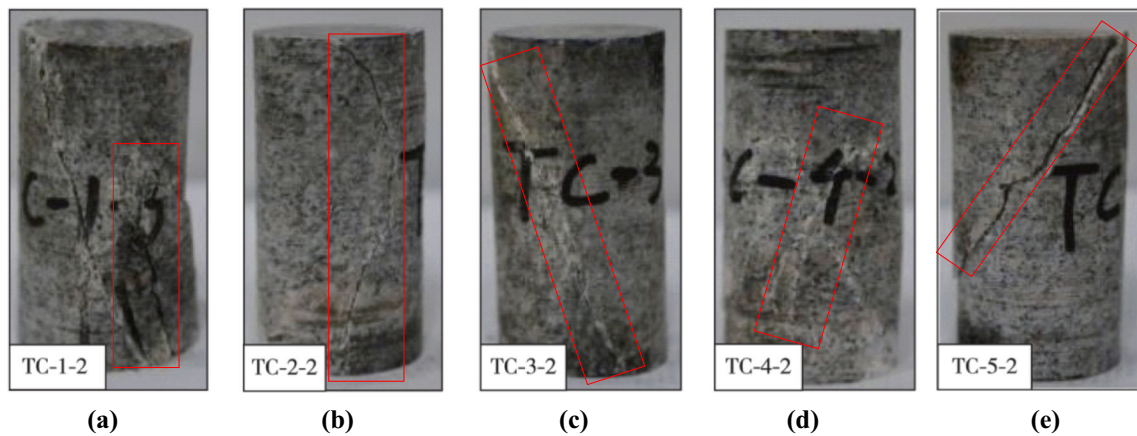


Fig. 13 The ultimate failure mode of the experimental specimen under different confining pressures. a 5 MPa. b 15 MPa. c 25 MPa. d 35 MPa. e 45 MPa

When the confining pressure increases to 45 MPa, the shear failure characteristics of the ECM become increasingly obvious, showing a macroshear zone with an angle of approximately 45° to the loading direction.

To verify the reliability of the calculation results, Fig. 13 shows the failure modes of the experimental specimens under the conditions of triaxial compression ($\sigma_3 = 5 \text{ MPa}, 15 \text{ MPa}, 25 \text{ MPa}, 35 \text{ MPa}$ and 45 MPa). When the confining pressure is 5 MPa and 15 MPa, the granite exhibits a split failure mode parallel to the loading direction. When the confining pressure is relatively high (i.e. 25 MPa, 35 MPa and 45 MPa), granite exhibits a shear failure mode at an angle with the loading direction. These test results are generally in agreement with the final failure mode of the ECM under different confining pressures, which further verifies the reliability and suitability

of using the ECM to study the mechanical properties of granite.

5 Conclusion

In this paper, an ECM consisting of the BPM and SJM is established, which can simultaneously reflect the structure and content of mineral granules in rock. Numerical simulation tests, such as direct tension, uniaxial compression and triaxial compression tests, were carried out based on the ECM and were compared with the experimental data for Beishan granite. The study explores the macroscopic nonlinear mechanical behaviour and fracture mechanism of brittle rock from the mesoscale and verifies the applicability and

reliability of the ECM. The main conclusions are summarized as follows.

1. The uniaxial tensile simulation test shows that the macroscopic fracture surface approximately perpendicular to the loading axis in rock is mainly composed of bond tension failure on the boundary of adjacent crystal granules.
2. In the simulation test of the uniaxial compression or low confining pressure triaxial compression, the macroscopic fracture surface approximately parallel to the loading axis in rock is mainly caused by the bond tension failure on the boundary of the adjacent crystal granules, which causes the rock to produce macroscopic splitting failure.
3. In the simulation test of high confining pressure triaxial compression, the macroscopic fracture surface penetrated at a certain angle with the loading axis in rock, mainly due to tension failure inside the crystal structure and bonding tension and shear failure on the boundary of the adjacent crystal granules, which causes the rock to produce macroscopic shear failure.
4. For hard and brittle rocks such as granite, the use of the ECM can reproduce a higher ratio of the uniaxial compressive strength to the uniaxial tensile strength of the rock, and its strength characteristics show obvious non-linear characteristics and meet the Hoek–Brown strength criterion. The rock strength and failure type obtained from the simulation are basically consistent with the test results, demonstrating the reliability of the ECM.

Acknowledgements The work was supported by the Fundamental Research Funds for the Central Universities (Grant No. FRF-TP-18-016A3) and the National Natural Science Foundation of China (Grant No. 51504016).

References

1. Cundall, P.A.; Strack, O.D.L.: A discrete numerical model for granular assemblies. *Geotechnique* **29**(1), 47–65 (1979)
2. Zhou, J.X.; Zhou, Y.; Gao, Y.T.: Effect mechanism of fractures on the mechanics characteristics of jointed rock mass under compression. *Arab. J. Sci. Eng.* **43**(7), 3659–3671 (2018)
3. Wu, T.H.; Gao, Y.T.; Zhou, Y.; et al.: Experimental and numerical study on the interaction between holes and fissures in rock-like materials under uniaxial compression. *Theor. Appl. Fract. Mech.* **106** (2020)
4. Yoon, J.: Application of experimental design and optimization to PFC model calibration in uniaxial compression simulation. *Int. J. Rock Mech. Min. Sci.* **44**(6), 871–889 (2007)
5. Potyondy, D.O.; Cundall, P.A.: A bonded-particle model for rock. *Int. J. Rock Mech. Min. Sci.* **41**(8), 1329–1364 (2004)
6. Li, J.W.; Zhou, Y.; Sun, W.; et al.: Effect of the interaction between cavity and flaw on the rock mechanical property under uniaxial compression. *Adv. Mater. Sci. Eng.* (2019), Article ID 1242141
7. Potyondy, D.O.: A flat-jointed bonded-particle material for rock. In: *Proceedings of 52nd US Rock Mech/Geomech Symposium* (Washington, USA, June 17–20, 2018), pp ARMA 18–1208 (2018)
8. Yoon, J.S.; Zang, A.; Stephansson, O.: Simulating fracture and friction of Aue granite under confined asymmetric compressive test using clumped particle model. *Int. J. Rock Mech. Min. Sci.* **49**(1), 68–83 (2012)
9. Zhou, Y.; Wu, S.C.; Gao, Y.T.; et al.: Macro and meso analysis of jointed rock mass triaxial compression test by using ERM technique. *J. Cent. South. Univ. T.* **21**(3), 1125–1135 (2014)
10. Zhou, Y.; Zhang, G.; Wu, S.C.; et al.: The effect of flaw on rock mechanical properties under the Brazilian test. *Kuwait. J. Sci.* **45**(2), 94–103 (2018)
11. Guo, W.H.; Chen, N.B.; Zhou, Y.; et al.: Meso research on the mechanical properties of rock specimens with double prefabricated circular holes based on digital image correlation. *Kuwait. J. Sci.* **47**(3), 2–14 (2020)
12. Park, J.W.; Song, J.J.: Numerical simulation of a direct shear test on a rock joint using a bonded-particle model. *Int. J. Rock Mech. Min. Sci.* **46**(8), 1315–1328 (2009)
13. Zhang, S.H.; Wu, S.C.; Duan, K.: Study on the deformation and strength characteristics of hard rock under true triaxial stress state using bonded-particle model. *Comput. Geotech.* **112**(8), 1–16 (2019)
14. Zhang, X.P.; Zhang, Q.; Wu, S.C.: Acoustic emission characteristics of the rock-like material containing a single flaw under different compressive loading rates. *Comput. Geotech.* **83**, 83–97 (2017)
15. Ding, X.B.; Zhang, L.Y.: A new contact model to improve the simulated ratio of unconfined compressive strength to tensile strength in bonded particle models. *Int. J. Rock Mech. Min. Sci.* **69**, 111–119 (2014)
16. Mehranpour, M.H.; Kulatilake, P.H.S.W.; Ma, X.; He, M.C.: Development of new three-dimensional rock mass strength criteria. *Rock Mech. Rock Eng.* **51**, 1–25 (2018)
17. Zhou, Y.; Chen, N.B.; Wu, S.C.; et al.: A flat-joint contact model and meso analysis on mechanical characteristics of brittle rock. *Kuwait. J. Sci.* **46**(3), 71–82 (2019)
18. Wu, S.C.; Xu, X.L.: A study of three intrinsic problems of the classic discrete element method using flat-joint model. *Rock Mech. Rock Eng.* **49**(5), 1813–1830 (2016)
19. Xu, X.L.; Wu, S.C.; Gao, Y.T.; et al.: Effects of micro-structure and micro-parameters on Brazilian tensile strength using flat-joint model. *Rock. Mech. Rock. Eng.* (2016)
20. Yang, X.X.; Qiao, W.G.: Numerical investigation of the shear behavior of granite materials containing discontinuous joints by utilizing the flat-joint model. *Comput. Geotech.* **104**(12), 69–80 (2018)
21. Cho, N.; Martin, C.D.; Sego, D.C.: A clumped particle model for rock. *Int. J. Rock Mech. Min. Sci.* **44**(7), 997–1010 (2007)
22. Li, P.F.; Zhao, X.G.; Guo, Z.; et al.: Variation of strength parameters of Beishan granite under triaxial compression. *Chin. J. Rock Mech. Eng.* **36**(7), 1599–1610 (2017)
23. Sun, X.; Li, E.B.; Duan, J.L.; et al.: Study on acoustic emission characteristics and damage evolution law of Beishan granite under triaxial compression. *Chin. J. Rock Mech. Eng.* **37**(Suppl 2), 4234–4244 (2018)
24. Wang, C.L.; Li, E.B.; Han, Y.; et al.: Study on mechanical characteristics and fracture evolution of Beishan granite under triaxial compression. *J. Forest. Eng.* **3**(4), 151–158 (2018)
25. Zhou, Y.; Gao, Y.T.; Wu, S.C.; et al.: An equivalent crystal model for mesoscopic behaviour of rock. *Chin. J. Rock Mech. Eng.* **34**(3), 511–519 (2015)
26. Potyondy, D.O.: *Smooth-Joint Model Version 2 (for PFC2D/3D Manual)*. Itasca Consulting Group, Minneapolis (2007)
27. Hoek, E.; Carranza-torres, C.T.; Corkum, B.: Hoek–Brown failure criterion-2002 edition. In: *Proceedings of the Fifth North American Rock Mechanics Symposium*. Toronto: [s.n.], pp. 267–273 (2002)

